Preparation, Biological Evaluation, and Pharmacokinetics of the Human Anti-*HER1* Monoclonal Antibody Panitumumab Labeled with ^{86}Y for Quantitative PET of Carcinoma

Tapan K. Nayak, Kayhan Garmestani, Kwamena E. Baidoo, Diane E. Milenic, and Martin W. Brechbiel

Radioimmune and Inorganic Chemistry Section, Radiation Oncology Branch, National Cancer Institute, National Institutes of Health, Bethesda, Maryland

Panitumumab, a human monoclonal antibody that binds to the epidermal growth factor receptor (*HER1*), was approved by the Food and Drug Administration in 2006 for the treatment of patients with *HER1*-expressing carcinoma. In this article, we describe the preclinical development of ^{86}Y-CHX-A″-diethylenetriaminepentaacetic acid (DTPA)-panitumumab for quantitative PET of *HER1*-expressing carcinoma. Panitumumab was conjugated to CHX-A″-DTPA and radiolabeled with ^{86}Y. In vivo biodistribution, PET, blood clearance, area under the curve, area under the moment curve, and mean residence time were determined for mice bearing *HER1*-expressing human colorectal (LS-174T), prostate (PC-3), and epidermoid (A431) tumor xenografts. Receptor specificity was demonstrated by coinjection of 0.1 mg of panitumumab with the radioimmunoconjugate. **Results:** ^{86}Y-CHX-A″-DTPA-panitumumab was routinely prepared with a specific activity exceeding 2 GBq/mg. Biodistribution and PET studies demonstrated a high *HER1*-specific tumor uptake of the radioimmunoconjugate. In mice bearing LS-174T, PC-3, or A431 tumors, the tumor uptake at 3 d was 34.6 ± 5.9, 22.1 ± 1.9, and 22.7 ± 1.7 percentage injected dose per gram (%ID/g), respectively. The corresponding tumor uptake in mice coinjected with 0.1 mg of panitumumab was 9.3 ± 1.5, 8.8 ± 0.9, and 10.0 ± 1.3 %ID/g, respectively, at the same time point, demonstrating specific blockage of the receptor. Normal organ and tumor uptake quantified by PET was closely related ($r^2 = 0.95$) to values determined by biodistribution studies. The LS-174T tumor had the highest area under the curve (96.8 ± 5.6 %ID·d·g^{-1}) and area under the moment curve (262.5 ± 14.9 %ID·d^2·g^{-1}); however, the tumor mean residence times were identical for all 3 tumors (2.7–2.8 d). **Conclusion:** This study demonstrates the potential of ^{86}Y-CHX-A″-DTPA-panitumumab for quantitative noninvasive PET of *HER1*-expressing tumors and represents the first step toward clinical translation.

The epidermal growth factor receptor (*HER1* or Erb1) is a transmembrane glycoprotein belonging to subclass I of the tyrosine kinase receptor superfamily (*1,2*). *HER1* signaling is firmly regulated in normal cells. The receptor is overexpressed in cancers ranging from lung to colorectal because of *HER1* gene amplification and anomalous expression and signaling in cancer cells. Overexpression of the receptor is associated with poor survival, disease progression, and resistance to conventional chemotherapy (*1,2*). To overcome resistance to chemotherapy and improve outcomes, *HER1*-targeted therapies are actively being developed. Two major classes of clinical therapies have been explored in the treatment of *HER1*-expressing cancer, with moderate success (*3,4*). These are anti-*HER1* monoclonal antibodies (mAbs) and *HER1*-specific tyrosine kinase inhibitors. Currently, 2 mAbs, cetuximab (Erbitux; ImClone and Bristol-Myers Squibb) and panitumumab (Vectibix; Amgen), are approved by the Food and Drug Administration.

Cetuximab is a chimeric anti-*HER1* IgG$_1$-isotype mAb indicated for use in patients with *HER1*-expressing metastatic colorectal cancer as a single-agent immunotherapy or in combination with irinotecan-based chemotherapy (*3,4*). The antitumor activity of cetuximab, however, requires high doses, and adverse reactions related to immune response and hypersensitivity to the antibody have been reported in approximately 19% of patients, with 3% of the patients experiencing severe reactions (*4–6*). The fully human anti-*HER1* mAb panitumumab was developed using Xeno-Mouse technology to improve therapeutic efficacy and decrease the potential of eliciting immune responses in patients (*7*). Panitumumab binds to the ligand-binding

domain (domain III) of *HER1* and is rapidly internalized, leading to downregulation of cell surface *HER1* in vitro and in vivo (*7,8*). In addition to inhibiting phosphorylation of *HER1* and mitogen-activated protein kinases or Akt, panitumumab also causes cell cycle arrest and inhibits tumor growth by suppressing the production of proangiogenic factors such as vascular endothelial growth factor and IL-8 by tumor cells (*7,8*).

Panitumumab was approved by the Food and Drug Administration in 2006 for the treatment of patients with *HER1*-expressing, metastatic colorectal carcinoma with disease progression during or after fluoropyrimidine-, oxiplatin-, and irinotecan-containing chemotherapy regimens (*9–11*). Panitumumab therapy is well tolerated in patients (*12,13*). A phase III trial of 463 patients with refractory metastatic colorectal cancer compared panitumumab plus best supportive care versus best supportive care alone. In the panitumumab group, as compared with best supportive care alone, a 46% reduction in the tumor-progression rate was reported (*14*). Panitumumab also significantly improved progression-free survival with manageable toxicity and was efficient in time-related endpoints. The clinical efficacy of panitumumab is currently being evaluated in patients with other types of cancers such as lung, breast, renal, head and neck, and ovarian (*10*).

A critical factor in screening patients for targeted therapy is evaluating the presence and amount of the specific target in the tumor and its relevance to the disease state. Initial clinical experience with both cetuximab and panitumumab therapy revealed that *HER1* levels detected by immunohistochemistry did not correlate with response to anti-*HER1* immunotherapy (*15,16*). Along with other pathologic procedures and tests, noninvasive nuclear imaging is often used to assess the status of the specific target. For instance, to assess the status of *HER1* expression and cetuximab distribution, cetuximab has been radiolabeled with radionuclides such as ^{99m}Tc and ^{111}In for SPECT (*17–20*), and cetuximab radiolabeled with ^{64}Cu and ^{89}Zr has been explored for PET (*21–24*). Panitumumab and cetuximab bind to different epitopes of *HER1*; therefore, a need to develop a panitumumab-specific imaging agent exists. Panitumumab conjugated with CHX-A″-diethylenetriaminepentaacetic acid (DTPA) and radiolabeled with ^{111}In has been extensively evaluated preclinically in this laboratory (*25*). In the report from that study, conjugating 1–2 molecules of CHX-A″-DTPA to panitumumab did not alter the binding affinity of panitumumab. Panitumumab was found to retain reactivity with *HER1* after modification with the CHX-A″-DTPA ligand and when radiolabeled with ^{111}In. Excellent tumor targeting by ^{111}In-CHX-A″-DTPA-panitumumab was demonstrated in vivo by direct quantitation of tumors and normal tissues in 5 tumor xenograft models. Considering the superiority of PET over single-photon scintigraphy, the development of a panitumumab-specific PET radioimmunoconjugate was deemed a worthwhile pursuit.

Of the numerous longer-lived positron-emitting radionuclides available for radioimmunoimaging—such as ^{124}I, ^{86}Y, ^{64}Cu, and ^{89}Zr—we selected ^{86}Y because of its appropriate half-life (14.7 h), suitability for internalizing mAbs, well-established chemistry, and availability (*26,27*). In addition to these attractive features, ^{86}Y can also serve as a surrogate marker for ^{90}Y-based radioimmunotherapy and peptide receptor radionuclide therapy (*28,29*). In a study describing ^{64}Cu-DOTA-panitumumab, the radioimmunoconjugate was successfully used to image *HER1*-expressing head and neck squamous cell tumor xenografts in mice (*30*).

In the present study, the preparation and evaluation of ^{86}Y-CHX-A″-DTPA-panitumumab for potential use in risk stratification and quantitative noninvasive imaging of *HER1* and assessment of panitumumab uptake in preclinical cancer models are described. To achieve this objective, ^{86}Y-CHX-A″-DTPA-panitumumab was assessed by in vivo biodistribution; PET and quantification; blood pharmacokinetics; and detailed analysis of area under the curve (AUC), area under the moment curve (AUMC), and mean residence time (MRT) for mice bearing *HER1*-expressing human colorectal (LS-174T), prostate (PC-3), and epidermoid (A431) tumor xenografts.

MATERIALS AND METHODS

Preparation of ^{86}Y-CHX-A″-DTPA-Panitumumab

Production and Purification of ^{86}Y. ^{86}Y was produced by the previously described ^{86}Sr(p,n)^{86}Y reaction, with minor modifications in the postirradiation processing of the SrCO$_3$ target (*27*). Briefly, the postirradiated SrCO$_3$ target was dissolved in 500 μL of 3 M ultrapure-grade nitric acid and heated to dryness twice; 300 μL of 8 M ultrapure-grade nitric acid were added to the residue to dissolve ^{86}Y. The mixture was allowed to cool in an ice bath to precipitate the strontium. The supernatant containing ^{86}Y was separated and heated to dryness. The ^{86}Y was extracted with 2 × 300 μL of 3 M nitric acid, loaded onto a preequilibrated 0.5-mL bed volume of strontium resin (EiChrom Industries), and eluted with 3 M nitric acid. The eluted ^{86}Y solution was heated to dryness, and the resultant ^{86}Y residue was extracted with 3 × 200 μL of 2 M nitric acid and loaded onto a preconditioned yttrium-selective RE-Spec resin column (EiChrom Industries). The ^{86}Y was eluted with 2 M nitric acid. The eluate containing ^{86}Y was heated to dryness, and the ^{86}Y residue was dissolved in 0.1 M nitric acid for radiolabeling procedures.

Radiolabeling CHX-A″-DTPA-Panitumumab with ^{86}Y. The bifunctional chelate, CHX-A″-DTPA, was conjugated to panitumumab as previously described (*25*). The chelate-to-protein ratio was determined using the Y(III)–Arsenazo(III) complex assay (*25,31*). For radiolabeling, a freshly prepared solution of ascorbic acid (50 μL, 220 μg/μL) was first added to the ^{86}Y solution (140–170 MBq in 0.1 M nitric acid, 500 μL) to prevent radiolysis of the mAb. The solution was neutralized to pH 5–6 by the addition of ammonium acetate buffer (50 μL 5 M, pH 7.0). CHX-A″-DTPA-panitumumab (50 μg in 0.15 M ammonium acetate) was added to the mixture, stirred briefly in a vortex mixer, and incubated at room temperature for 30 min. The reaction was quenched by the

addition of ethylenediaminetetraacetic acid solution (4 µL, 0.1 M). The radiolabeled product was purified using a PD-10 desalting column (GE Healthcare). Size-exclusion high-performance liquid chromatography using a TSK-3000 column (Toso-Haas) was performed to ascertain the purity of the radioimmunoconjugate using previously described solvent conditions and analysis parameters (27).

Cell Lines

HER1-expressing human LS-174T, PC-3, and A431 carcinoma cells (American Type Culture Collection) were grown as a monolayer at 37°C, in a humidified atmosphere of 5% CO_2 and 95% air. LS-174T and A431 cells were cultured in Dulbecco's minimal essential medium containing 10% FetaPLEX (Gemini Bio-Products) and 10 mM glutamine solution. PC-3 cells were cultured in RPMI 1640 medium containing FetaPLEX (10%). Medium and supplements were obtained from Quality Biologicals, Invitrogen, and Lonza.

In Vitro Evaluations

In radioligand cell-binding studies, the immunoreactivity of the ⁸⁶Y-CHX-A″-DTPA-panitumumab was determined using a *HER1*-positive human A431 fixed-cell radioimmunoassay (25).

Animal and Tumor Models

Female athymic *nu/nu* mice (Charles River Laboratory) were injected subcutaneously with 2×10^6 cells of each cell line (200 µL

of medium containing 20% Matrigel [BD Biosciences]). In vivo experiments were performed when the tumor diameter reached 0.5–0.7 cm. Tumor necrosis was examined by hematoxylin and eosin staining, and *HER1* expression was confirmed by immunohistochemistry on selected formalin-fixed, paraffin-embedded tumors. Tumors were carefully removed and fixed in 4% buffered paraformaldehyde solution and incubated overnight at 4°C. After the incubation period, the fixed tumor was washed with phosphate-buffered saline solution and stored in 70% ethanol solution at 4°C before paraffin-embedding. For immunohistochemistry experiments, panitumumab was used as the primary antibody to determine the available binding sites on the tumor sections. Immunohistochemistry was performed and analyzed at Histoserv, Inc. All animal studies were performed in accordance with the National Institutes of Health guidelines for the humane use of animals, and all procedures were reviewed and approved by the National Cancer Institute Animal Care and Use Committee.

In Vivo Evaluations

Biodistribution and Pharmacokinetic Studies. Female athymic mice bearing human LS-174T, PC-3, or A431 tumor xenografts were injected intravenously via the tail with 0.4–0.6 MBq (less than 5 µg) of ⁸⁶Y-CHX-A″-DTPA-panitumumab. To determine *HER1* specificity, panitumumab (0.1 mg) was coinjected with the radiotracer in an additional set of mice bearing each of the tumor xenografts. At the desired times, the animals were sacrificed by
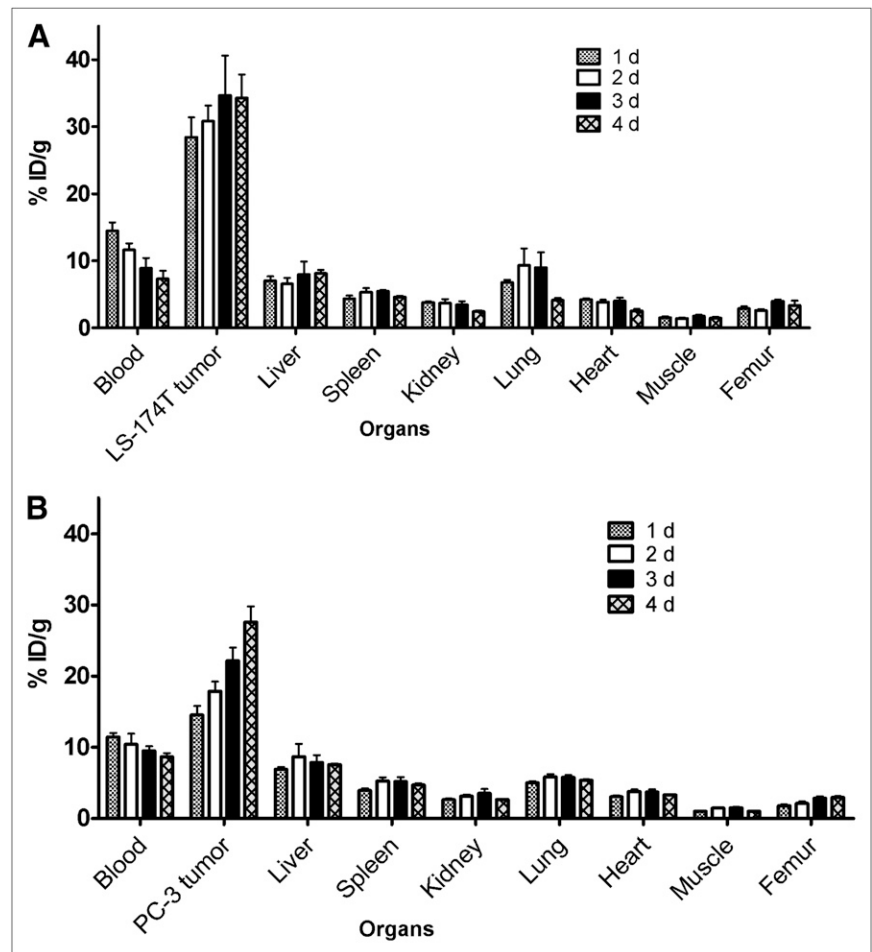

FIGURE 1. Biodistribution of ⁸⁶Y-CHX-A″-DTPA-panitumumab in selected organs of female athymic (NCr) *nu/nu* mice bearing human LS-174T (A) and PC-3 (B) tumor xenografts. Biodistribution data were obtained at 1, 2, 3, and 4 d after intravenous injection of ⁸⁶Y-CHX-A″-DTPA-panitumumab. All values are expressed as %ID/g. Data represent mean value ± SEM from at least 4 determinations.

CO_2 inhalation. Tumor, blood, and selected normal organs were harvested and wet-weighed, and the radioactivity was measured in a Wizard 1480 γ-counter (PerkinElmer). The percentage injected dose per gram (%ID/g) of tissue was calculated by comparison with standards representing 10% of the injected dose per animal.

Blood pharmacokinetics of the ^{86}Y-CHX-A″-DTPA-panitumumab was determined as previously described (27). The percentage injected dose per milliliter of blood was calculated for each of the samples and clearance determined by biphasic nonlinear regression analysis using GraphPad Prism (version 5; GraphPad Software). Noncompartmental pharmacokinetics were determined for AUC, AUMC, and MRT using trapezoidal integration analysis (32).

PET Studies. Small-animal PET studies were performed using the Advanced Technology Laboratory Animal Scanner at the National Institute of Biomedical Imaging and Bioengineering, National Institutes of Health. Whole-body imaging studies (6 bed positions, total acquisition time of 1 h per mouse) were performed on mice anesthetized with 1.5%−1.7% isoflurane on a temperature-controlled bed. Female athymic mice bearing LS-174T, A431, and PC-3 tumor xenografts ($n = 3$) were injected intravenously with 1.8–2.0 MBq of ^{86}Y-CHX-A″-DTPA-panitumumab. To determine *HER1* specificity, excess panitumumab (0.1 mg) was coinjected with the radiotracer. ^{86}Y cylinder phantoms were imaged during each imaging session for normalization and quantitative analysis. The energy window for PET acquisition of ^{86}Y was set between 400 and 700 keV. The imaging data were reconstructed using a 2-dimensional Fourier rebinned ordered-subsets expectation maximization method with scatter correction (linear background subtraction). Additional dead time, decay, and background corrections were applied for quantitative analysis. The reconstructed images were processed and analyzed using the AMIDE: A Medical Image Data Examiner software program. To minimize spillover effects, regions of interest were drawn to enclose approximately 80%−90% of the organ of interest to avoid the edges. To minimize partial-volume effects caused by nonuniform distribution of the radioactivity in the containing volume, smaller regions of interest were consistently drawn to enclose the organ. After the imaging studies, the mice were euthanized and in vivo biodistribution studies were performed to determine the correlation between %ID/cm^3 as assessed by PET and %ID/g obtained from biodistribution studies.

Statistical Analysis

All numeric data were expressed as the mean of the values ± SEM. GraphPad Prism, version 5, was used for statistical analysis. A *P* value of less than 0.05 was considered statistically significant.

RESULTS

Radiochemistry and In Vitro Evaluations

Panitumumab was modified with the acyclic ligand CHX-A″-DTPA at a 10:1 molar excess of chelate to protein, yielding a final chelate-to-protein ratio of 1.6 chelate molecules per protein molecule. The ^{86}Y-CHX-A″-DTPA-panitumumab conjugate was successfully prepared, with the radiochemical yields ranging from 60% to 75% and specific activity exceeding 2 GBq/mg. The ^{86}Y-CHX-A″-DTPA-panitumumab conjugate demonstrated

excellent in vitro receptor specificity, as exhibited by an immunoreactivity (%) of 73.51 ± 4.76 and nonspecific binding (%) of 3.79 ± 1.69 ($n = 4$) on fixed A431 cells. On high-performance liquid chromatography analysis, the radioimmunoconjugate exhibited excellent stability after storage in the refrigerator at 4°C for 1 d and retained the immunoreactivity (Supplemental Fig. 1; supplemental
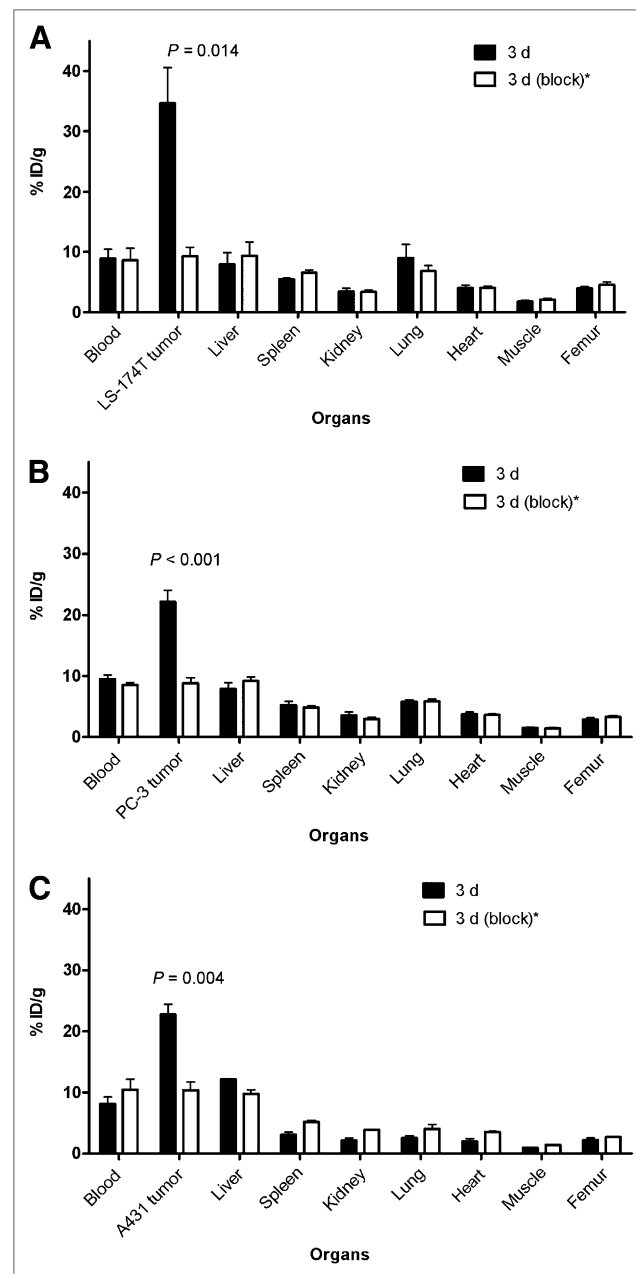

FIGURE 2. Receptor-mediated uptake of ^{86}Y-CHX-A″-DTPA-panitumumab in selected organs of female athymic (NCr) *nu/nu* mice bearing human LS-174T (A), PC-3 (B), and A431 (C) tumor xenografts. Biodistribution data were obtained at 3 d after injection. All values are expressed as %ID/g. Data represent mean value ± SEM from at least 3 determinations. *Receptor blocking studies were performed by coinjecting 0.1 mg of panitumumab with radiotracer.

materials are available online only at http://jnm.snmjournals. org).

In Vivo Evaluations

Biodistribution Studies. In mice bearing LS-174T tumor xenografts, an approximately 50% decrease in the blood-pool activity was observed over 4 d (14.47 ± 1.28 %ID/g at 1 d to 7.30 ± 1.21 %ID/g at 4 d) (Fig. 1A). An opposite trend was observed in tumor uptake, with the %ID/g of 28.43 ± 2.93 observed at 1 d increasing to 34.30 ± 3.47 %ID/g at 4 d after injection (Fig. 1A). The tumor-to-blood ratio increased more than 2-fold from 2.0 at 1 d to 4.7 at 4 d after injection. In mice bearing PC-3 xenografts, the blood-pool activity of the radiotracer decreased from 11.45 ± 0.56 %ID/g at 1 d to 8.66 ± 0.52 %ID/g at 4 d after injection (Fig. 1B). In contrast, an approximately 50% increase in the tumor uptake was observed from a 1- to 4-d period (14.53 ± 1.29 %ID/g at 1 d to 27.61 ± 2.81 %ID/g at 4 d after injection). The tumor-to-blood ratios in mice bearing PC-3 xenografts were relatively lower than those observed in mice bearing LS-174T xenografts (1.27 at 1 d after injection to 3.18 at 4 d after injection) because of the slower localization of the radiotracer in PC-3 xenografts than in the LS-174T xenografts.

The ^{86}Y-CHX-A″-DTPA-panitumumab uptake in all the tumor models was *HER1*-mediated, as demonstrated by the receptor-blocking experiments performed by coinjecting 0.1 mg of panitumumab (Fig. 2). In mice bearing LS-174T (Fig. 2A), PC-3 (Fig. 2B), or A431 (Fig. 2C) tumors, the tumor %ID/g at 3 d was 34.65 ± 5.9, 22.1 ± 1.9, and 22.74 ± 1.7, respectively. The corresponding tumor %ID/g in mice coinjected with 0.1 mg of panitumumab was 9.28 ± 1.5, 8.80 ± 0.9, and 10.04 ± 1.3, respectively, at the same time, thus demonstrating the specificity of the radioimmunoconjugate. Immunohistochemistry revealed varied levels of *HER1* expression in all tumors. A431 tumors had the highest expression levels of *HER1* (Table 1). LS-174T tumor sections had the weakest *HER1* staining patterns ($+$), A431 tumor sections had the strongest *HER1* staining patterns ($+++$), and PC-3 tumor sections demonstrated either a weak ($+$) or a moderate ($++$) *HER1* staining pattern.

Pharmacokinetic Analysis. From the blood clearance studies, the half-life of the α-phase of the biphasic blood clearance ranged from 2.7 ± 1.2 h for mice bearing PC-3 xenografts to 3.7 ± 1.7 h for mice bearing LS-174T xenografts (Table 1). The half-life of the β-phase was identical for all 3 tumor models. The mice bearing LS-174T tumors had the highest AUC (96.8 ± 5.6 %ID·d·g^{-1}) and AUMC (262.5 ± 14.9 %ID·d^2·g^{-1}). The tracer accumulation was significantly higher in LS-174T tumors ($P < 0.05$) than in A431 and PC-3 tumors, as shown in Table 1. However, the tumor MRTs were identical for all 3 tumors (2.7–2.8 d). The LS-174T tumor AUC$_{[0 \rightarrow 4\ d]}$:blood AUC$_{[0 \rightarrow 4\ d]}$ ratio of 3:1 was nearly 1.5 times greater than the PC-3 and A431 tumor AUC$_{[0 \rightarrow 4\ d]}$:blood AUC$_{[0 \rightarrow 4\ d]}$ ratio of 2.0 (Table 1).

PET Studies. The linearity of the PET-assessed concentration versus the radioactivity concentration measured in a Capintec CRC-127R dose calibrator was $r^2 = 0.99$ in the radioactivity range of 0.03–3.63 MBq/mL of ^{86}Y solution from cylindric phantom studies.

Small-animal PET studies were performed in female athymic mice bearing LS-174T (Figs. 3A−3B), A431 (Figs. 3C−3D), and PC-3 (Supplemental Fig. 2) xenografts injected with 1.8–2.0 MBq of ^{86}Y-CHX-A″-DTPA-panitumumab or ^{86}Y-CHX-A″-DTPA-panitumumab coinjected with 0.1 mg of panitumumab. The LS-174T (Fig. 3A) and A431 (Fig. 3C) tumors were clearly visualized in maximum-intensity projections (top) and transverse slices (bottom) of mice imaged from 0.5 to 3 d after injection of the radioimmunoconjugate. The tumor-to-background

TABLE 1. Pharmacokinetic Characteristics of ^{86}Y-CHX-A″-DTPA-Panitumumab in Female Athymic (NCr) *nu/nu* Mice

Pharmacokinetic characteristic	LS-174T	PC-3	A431
Relative in vitro expression*	62.5	150.9	2,072.2
Relative in vivo expression	+	+-++	+++
Blood clearance (h)			
Half-life of α-phase	3.7 ± 1.7	2.7 ± 1.2	3.1 ± 1.3
Half-life of β-phase	58.4 ± 15.3	69.2 ± 14.4	73.9 ± 13.0
Blood AUC$_{[0 \rightarrow 4]}$ (%ID·d·g^{-1})	31.4 ± 1.5	30.0 ± 2.2	32.3 ± 2.2
Tumor AUC$_{[0 \rightarrow 4]}$ (%ID·d·g^{-1})	96.8 ± 5.6	61.1 ± 3.7	65.3 ± 3.2
Tumor PET AUC$_{[0 \rightarrow 3]}$ (%ID·d/cm^3)	72.4 ± 5.3	38.8 ± 2.8	51.2 ± 2.9
Tumor PET AUC$_{[0 \rightarrow 3]}$ (%ID·d/cm^3)†	23.2 ± 3.7	21.7 ± 1.0	26.3 ± 1.9
Tumor AUC$_{[0 \rightarrow 4]}$:blood AUC$_{[0 \rightarrow 4]}$	3.1	2.0	2.0
Tumor AUMC$_{[0 \rightarrow 4]}$ (%ID·d^2·g^{-1})	262.5 ± 14.9	171.9 ± 10.3	179.9 ± 8.8
Tumor MRT (d)	2.7	2.8	2.7

*Mean fluorescence intensity from flow cytometry cell-binding studies as measure of relative in vitro expression.

†Receptor-blocking studies performed by coinjecting 0.1 mg of panitumumab with radiotracer. Values obtained from blocking studies were significantly lower than those from unblocked studies ($P < 0.05$), demonstrating receptor-mediated accumulation in tumors.

Data are adapted from Ray et al. (*25*). Data represent mean values from 3 to 6 determinations.
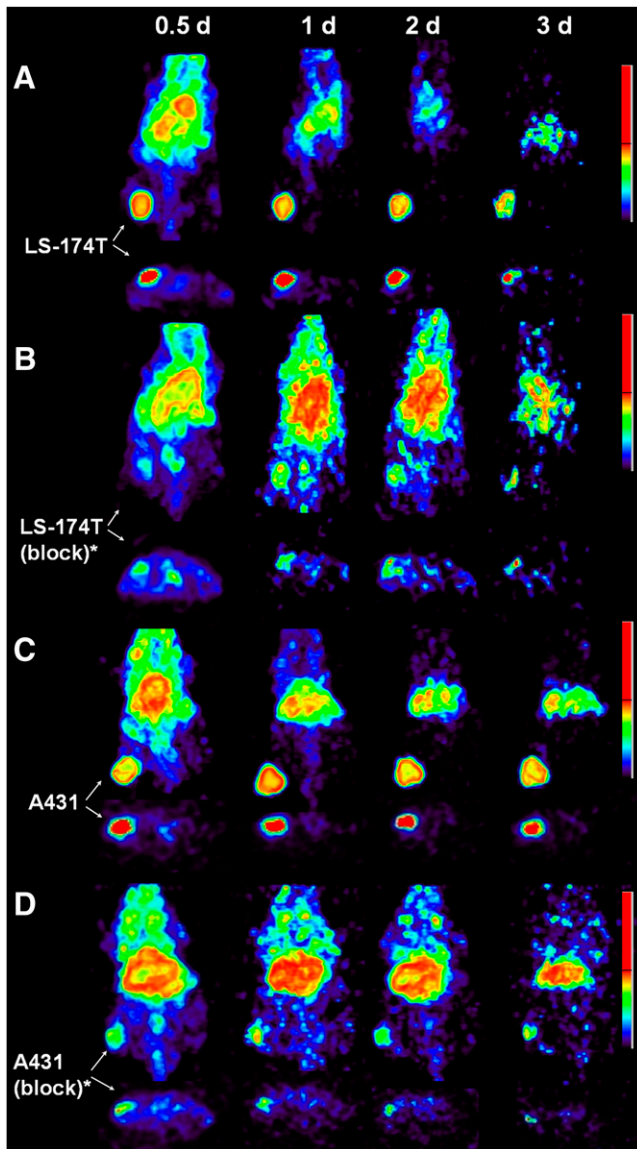
FIGURE 3. Representative reconstructed and processed maximum-intensity projections (top) and transverse slices (bottom) of female athymic (NCr) *nu/nu* mouse bearing human LS-174T (A and B) and A431 (C and D) tumor xenografts. Mice in A and C were injected intravenously via tail vein with 1.8–2.0 MBq of ^{86}Y-CHX-A″-DTPA-panitumumab, and mice in B and D were coinjected intravenously via tail vein with 1.8–2.0 MBq of ^{86}Y-CHX-A″-DTPA-panitumumab and 0.1 mg of panitumumab for blocking *HER1*. Tumors are indicated with white arrows. Scale represents percentage of maximum and minimum threshold intensity. *Receptor blocking studies were performed by coinjecting 0.1 mg of panitumumab with radiotracer.

ratios improved over the period, mostly because of the decrease of radioactivity in blood, liver, and background, whereas the tumor uptake increased. In contrast, when 0.1 mg of panitumumab was coinjected with the radiotracer, the tumors were poorly visualized because of receptor-specific blockage, demonstrating the *HER1*-specificity of

^{86}Y-CHX-A″-DTPA-panitumumab (Figs. 3B and 3D). No significant differences were found in the liver and muscle uptake of mice injected with ^{86}Y-CHX-A″-DTPA-panitumumab and mice coinjected with 0.1 mg of cold panitumumab (Fig. 4A). As shown in Figure 4B, the quantitated tumor uptake of mice injected with ^{86}Y-CHX-A″-DTPA-panitumumab and mice injected with ^{86}Y-CHX-A″-DTPA-panitumumab plus 0.1 mg of cold panitumumab was significantly different at 1, 2, and 3 d after injection. However, the tumor uptake was not significantly different at 0.5 d after injection ($P = 0.08$ for LS-174T, $P = 0.10$ for A431, and $P = 0.09$ for PC-3 tumors). For mice bearing LS-174T tumors, the PET-assessed tumor $AUC_{[0\rightarrow 3\ d]}$ of mice injected with ^{86}Y-CHX-A″-DTPA-panitumumab was 3.1 times greater than that of mice coinjected with 0.1 mg of panitumumab (Table 1). The PET-assessed tumor $AUC_{[0\rightarrow 3\ d]}$ of mice bearing PC-3 and A431 tumors injected with ^{86}Y-CHX-A″-DTPA-panitumumab was 1.6 and 1.9 times, respectively, greater than that of groups coinjected with 0.1 mg of panitumumab. In fact, a statistically significant difference was observed in tumor-bearing mice injected with ^{86}Y-CHX-A″-DTPA-panitumumab alone and ^{86}Y-CHX-A″-DTPA-panitumumab coinjected with 0.1 mg of panitumumab. The liver, tumor, and muscle uptake quantified by PET at all times was closely related ($r^2 = 0.95$, $P = 0.87$, $n = 30$) to values determined by in vivo biodistribution studies (Fig. 4).

DISCUSSION

Advances in genomics and proteomics are revolutionizing cancer therapy. Significant progress has been made in the development of targeted cancer therapy, wherein the drug specifically targets a unique protein or gene product overexpressed in tumors. Traditionally, in vitro assays of tumor biopsy material are used to evaluate the expression of the tumor biomarker that is vital for selecting patients for targeted therapy. Complementary to biopsy assays, molecular imaging has been used to measure regional tumor target expression and therefore select patients for appropriate cancer therapy and to evaluate treatment response (*33,34*).

Toward this end, ^{86}Y-CHX-A″-DTPA-panitumumab was explored as a noninvasive molecular imaging tool for selecting patients for *HER1*-targeted panitumumab therapy and for dosimetry assessment for possible targeted ^{90}Y therapy.

^{86}Y-CHX-A″-DTPA-panitumumab was routinely prepared with a specific activity exceeding 2 GBq/mg (0.3 GBq/nmol) and radiochemical yields exceeding 60%. When compared with ^{64}Cu-DOTA mAb and ^{89}Zr-desferrioxamine-mAb, ^{86}Y-CHX-A″-DTPA-mAb offers a viable alternative because of its greater in vivo stability, greater tumor-to-background ratios, and significant ease of preparation, as demonstrated by this study.
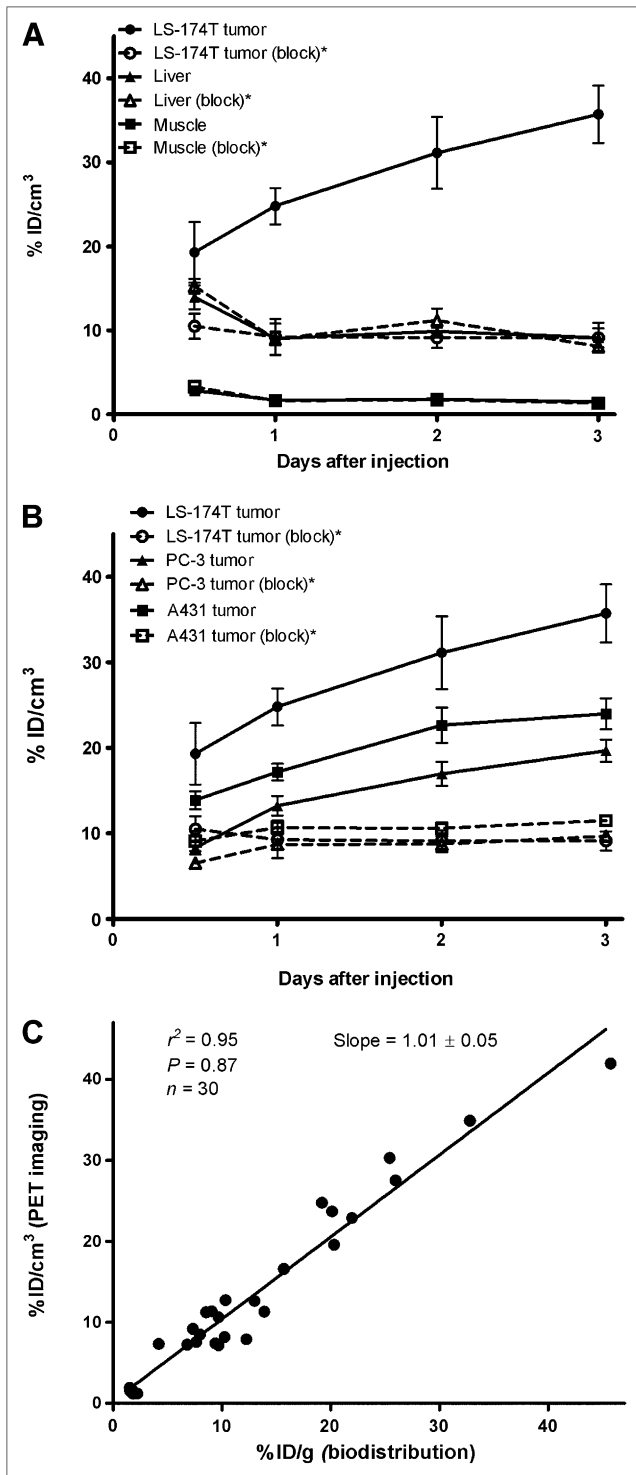
FIGURE 4. (A) Time–activity curve and uptake values of [86]Y-CHX-A″-DTPA-panitumumab in selected organs of female athymic (NCr) *nu/nu* mice bearing human LS-174T xenografts assessed through quantitative small-animal PET. (B) Comparative time–activity curves of [86]Y-CHX-A″-DTPA-panitumumab in female athymic (NCr) *nu/nu* mice bearing LS-174T, A431, and PC-3 tumor xenografts. (C) Correlation between organ %ID/g values assessed through in vivo biodistribution studies and quantitative small-animal PET. All uptake values derived from PET studies are expressed as

The biodistribution, noncompartmental pharmacokinetics, and imaging data reveal *HER1*-mediated uptake and accumulation in *HER1*-expressing tumor xenografts (Figs. 1–4; Table 1). [86]Y-CHX-A″-DTPA-panitumumab had a relatively longer half-life and slower blood clearance than did radiolabeled cetuximab (*20*). The biodistribution and blood pharmacokinetics of [86]Y-CHX-A″-DTPA-panitumumab were similar to those of ^{111}In-CHX-A″-DTPA-panitumumab, except for lung and femur uptake. These minor differences in [111]In- and [86]Y-labeled mAb may be attributed to radiometabolites, as previously observed (*27*). Data on blood clearance and tumor residence time as obtained in this study should prove useful for dosing in panitumumab-related therapies.

Studies have concluded that ^{64}Cu-DOTA-cetuximab could be used to detect and quantify *HER1* expression and therefore monitor therapeutic response (*22,23*). However, no correlation among relative in vitro expression determined by flow cytometry, relative ex vivo expression determined by immunohistochemistry, and tumor uptake and accumulation (Table 1) was found in the studies presented here. In fact, the cell line demonstrating the lowest *HER1* expression (LS-174T) resulted in the highest tumor uptake and accumulation (Table 1; Figs. 1–4). A recent study performed with [89]Zr-labeled cetuximab also found no correlation between ex vivo expression of *HER1* and radioimmunoconjugate uptake (*21*). The report describing ^{64}Cu-DOTA-panitumumab also described discrepancies in tumor uptake and ex vivo *HER1* expression levels determined by immunohistochemistry (*30*). This apparent dichotomy can be explained by the fact that in vivo accretion in tumor is actually dependent on many physiologic factors including tumor vasculature, blood flow, tumor interstitial pressure, and antigen shedding. Above all else, there are clearly obvious differences between the in vivo and the in vitro milieu of the surrounding environment ranging from cell-to-cell interactions to growth factors and such (*35*). Therefore, to correlate *HER1* expression and tumor uptake, further studies are warranted. In vivo determination of the distribution of the targeted biomarker and simultaneous determination of its true availability to the drug for therapy provide an extremely important metric that conveys the suitability of the patient for therapy and profoundly personalizes the treatment to the patient. The added advantage is that this information is obtained noninvasively. PET with [86]Y-CHX-A″-DTPA-panitumumab may have an extremely useful role in the selection of patients for panitumumab-related therapy because it would indicate *HER1* accessibility to the antibody. However, it is also possible that [86]Y-CHX-A″-DTPA-panitumumab imaging by itself may not predict the response to therapy but it

%ID/cm³. Data represent mean value ± SEM from 3 determinations. *Receptor blocking studies performed by coinjecting 0.1 mg of panitumumab with radiotracer.

indicates only how much panitumumab reaches the tumor. ^{86}Y-CHX-A″-DTPA-panitumumab imaging does not reveal the status of v-kis-ras2 Kirsten rat sarcoma viral oncogene mutations, which is critical for response to *HER1* immunotherapy (*36–38*). Thus, the role of panitumumab imaging may be complementary and best used together with assays to determine v-kis-ras2 Kirsten rat sarcoma viral oncogene mutations and *HER1* gene amplification and polymorphism (*36–38*).

The available radionuclides for PET radioimmunoimaging are ^{124}I, ^{64}Cu, ^{89}Zr, and ^{86}Y. Each of these radionuclides has its own specific drawback (*26*). Panitumumab is rapidly internalized; therefore, we anticipate that ^{124}I will be dehalogenated rapidly in vivo and result in poor tumor-to-background ratio. ^{64}Cu-1,4,8,11-tetraazacyclotetradecane-*N,N′,N″,N′″*-tetraacetic acid-1A3 has previously been reported for clinical PET of metastatic colorectal cancer (*39,40*). Although all 17 primary and recurrent sites were clearly visualized in patients, only 23 of 39 metastatic sites (59%) were detected (*40*). The detection of lung and liver metastasis was seriously hindered by nonspecific uptake in the liver and the blood because of dissociation of the ^{64}Cu from the currently used chelates for radiolabeling mAbs. ^{89}Zr is an attractive positron emitter because of its longer half-life; however, preparation of ^{89}Zr-labeled mAbs is a multistep, tedious process and ^{89}Zr has been shown to dissociate from the currently used chelates and to localize in the bone thereafter (*24*). On the other hand, the chelation chemistry and the preparation of yttrium-labeled mAbs for clinical use are well established. Although the half-life of ^{86}Y is slightly longer than that of ^{64}Cu, the abundance of positrons is also almost twice that of ^{64}Cu. With these advantages over ^{64}Cu, we anticipate much lower amounts of ^{86}Y will be required for quantitative immunoPET at 2 d after injection. On the basis of those previous studies performed with ^{64}Cu-labeled mAb (*39,40*), we anticipate that injection of between 0.18 and 0.37 GBq of the radioimmunoconjugate will result in useful quantitative images up to 2–3 d after injection.

We are currently performing radioimmunotherapy of *HER1*-expressing solid tumors with ^{90}Y-CHX-A″-DTPA-panitumumab. Therefore, ^{86}Y-CHX-A″-DTPA-panitumumab serves as a surrogate PET marker for dosimetry and selection of subjects for ^{90}Y CHX-A″-DTPA-panitumumab radioimmunotherapy of *HER1*-expressing carcinoma. To achieve the long-term goal of clinical translation of ^{86}Y-CHX-A″-DTPA-panitumumab, PET/CT and MRI studies are currently being performed with mice bearing orthotopic and disseminated tumors.

CONCLUSION

^{86}Y-CHX-A″-DTPA-panitumumab has been prepared with high specific activity. The utility of the radioimmunoconjugate for noninvasive PET of *HER1*-expressing tumors in preclinical models has been demonstrated. ^{86}Y-

CHX-A″-DTPA-panitumumab as a radiotracer may be used for the assessment of panitumumab uptake, which may be important for risk stratification, patient screening, and appropriate dosage selection. This preclinical study elucidating the biologic and pharmacokinetic characteristics of ^{86}Y-CHX-A″-DTPA-panitumumab represents the first step toward the clinical translation.

REFERENCES

1. Hynes NE, Lane HA. ERBB receptors and cancer: the complexity of targeted inhibitors. *Nat Rev Cancer.* 2005;5:341–354.
2. Burgess AW. EGFR family: structure physiology signalling and therapeutic targets. *Growth Factors.* 2008;26:263–274.
3. Harari PM. Epidermal growth factor receptor inhibition strategies in oncology. *Endocr Relat Cancer.* 2004;11:689–708.
4. Mendelsohn J, Baselga J. Epidermal growth factor receptor targeting in cancer. *Semin Oncol.* 2006;33:369–385.
5. Patel DD, Goldberg RM. Cetuximab-associated infusion reactions: pathology and management. *Oncology (Williston Park).* 2006;20:1373–1382; discussion 1382, 1392–1374, 1397.
6. Messersmith WA, Hidalgo M. Panitumumab, a monoclonal anti epidermal growth factor receptor antibody in colorectal cancer: another one or the one? *Clin Cancer Res.* 2007;13:4664–4666.
7. Yang XD, Jia XC, Corvalan JR, Wang P, Davis CG. Development of ABX-EGF, a fully human anti-EGF receptor monoclonal antibody, for cancer therapy. *Crit Rev Oncol Hematol.* 2001;38:17–23.
8. Lynch DH, Yang XD. Therapeutic potential of ABX-EGF: a fully human anti-epidermal growth factor receptor monoclonal antibody for cancer treatment. *Semin Oncol.* 2002;29(1, suppl 4):47–50.
9. Mano M, Humblet Y. Drug insight: panitumumab, a human EGFR-targeted monoclonal antibody with promising clinical activity in colorectal cancer. *Nat Clin Pract Oncol.* 2008;5:415–425.
10. Wu M, Rivkin A, Pham T. Panitumumab: human monoclonal antibody against epidermal growth factor receptors for the treatment of metastatic colorectal cancer. *Clin Ther.* 2008;30:14–30.
11. Giusti RM, Shastri KA, Cohen MH, Keegan P, Pazdur R. FDA drug approval summary: panitumumab (Vectibix). *Oncologist.* 2007;12:577–583.
12. Heun J, Holen K. Treatment with panitumumab after a severe infusion reaction to cetuximab in a patient with metastatic colorectal cancer: a case report. *Clin Colorectal Cancer.* 2007;6:529–531.
13. Nielsen DL, Pfeiffer P, Jensen BV. Six cases of treatment with panitumumab in patients with severe hypersensitivity reactions to cetuximab. *Ann Oncol.* 2009; 20:798.
14. Van Cutsem E, Peeters M, Siena S, et al. Open-label phase III trial of panitumumab plus best supportive care compared with best supportive care alone in patients with chemotherapy-refractory metastatic colorectal cancer. *J Clin Oncol.* 2007;25:1658–1664.
15. Hecht JR, Patnaik A, Berlin J, et al. Panitumumab monotherapy in patients with previously treated metastatic colorectal cancer. *Cancer.* 2007;110:980–988.
16. Chung KY, Shia J, Kemeny NE, et al. Cetuximab shows activity in colorectal cancer patients with tumors that do not express the epidermal growth factor receptor by immunohistochemistry. *J Clin Oncol.* 2005;23:1803–1810.
17. Wen X, Wu QP, Ke S, et al. Conjugation with ^{111}In-DTPA-poly(ethylene glycol) improves imaging of anti-EGF receptor antibody C225. *J Nucl Med.* 2001;42: 1530–1537.

18. Schechter NR, Wendt RE, 3rd, Yang DJ, et al. Radiation dosimetry of [99mTc]-labeled C225 in patients with squamous cell carcinoma of the head and neck. *J Nucl Med.* 2004;45:1683–1687.

19. Barrett T, Koyama Y, Hama Y, et al. In vivo diagnosis of epidermal growth factor receptor expression using molecular imaging with a cocktail of optically labeled monoclonal antibodies. *Clin Cancer Res.* 2007;13:6639–6648.

20. Milenic DE, Wong KJ, Baidoo KE, et al. Cetuximab: preclinical evaluation of a monoclonal antibody targeting EGFR for radioimmunodiagnostic and radio-immunotherapeutic applications. *Cancer Biother Radiopharm.* 2008;23:619–631.

21. Aerts HJ, Dubois L, Perk L, et al. Disparity between in vivo EGFR expression and [89Zr]-labeled cetuximab uptake assessed with PET. *J Nucl Med.* 2009;50:123–131.

22. Cai W, Chen K, He L, Cao Q, Koong A, Chen X. Quantitative PET of EGFR expression in xenograft-bearing mice using [64Cu]-labeled cetuximab, a chimeric anti-EGFR monoclonal antibody. *Eur J Nucl Med Mol Imaging.* 2007;34:850–858.

23. Eiblmaier M, Meyer LA, Watson MA, Fracasso PM, Pike LJ, Anderson CJ. Correlating EGFR expression with receptor-binding properties and internalization of [64Cu]-DOTA-cetuximab in 5 cervical cancer cell lines. *J Nucl Med.* 2008;49:1472–1479.

24. Perk LR, Visser GW, Vosjan MJ, et al. [89Zr] as a PET surrogate radioisotope for scouting biodistribution of the therapeutic radiometals [90Y] and [177Lu] in tumor-bearing nude mice after coupling to the internalizing antibody cetuximab. *J Nucl Med.* 2005;46:1898–1906.

25. Ray G, Baidoo K, Wong K, et al. Preclinical evaluation of a monoclonal antibody targeting the epidermal growth factor receptor as a radioimmunodiagnostic and radioimmunotherapeutic agent. *Br J Pharmacol.* 2009;157:1541–1548.

26. Nayak TK, Brechbiel MW. Radioimmunoimaging with longer-lived positron-emitting radionuclides: potentials and challenges. *Bioconjug Chem.* 2009;20:825–841.

27. Garmestani K, Milenic DE, Plascjak PS, Brechbiel MW. A new and convenient method for purification of [86Y] using a Sr(II) selective resin and comparison of biodistribution of [86Y] and [111In] labeled Herceptin. *Nucl Med Biol.* 2002;29:599–606.

28. Palm S, Enmon RM Jr, Matei C, et al. Pharmacokinetics and biodistribution of [86Y]-trastuzumab for [90Y] dosimetry in an ovarian carcinoma model: correlative microPET and MRI. *J Nucl Med.* 2003;44:1148–1155.

29. Helisch A, Forster GJ, Reber H, et al. Pre-therapeutic dosimetry and biodistribution of [86Y]-DOTA-Phe1-Tyr3-octreotide versus [111In]-pentetreotide in patients with advanced neuroendocrine tumours. *Eur J Nucl Med Mol Imaging.* 2004;31:1386–1392.

30. Niu G, Li Z, Xie J, Le QT, Chen X. PET of EGFR antibody distribution in head and neck squamous cell carcinoma models. *J Nucl Med.* 2009;50:1116–1123.

31. Pippin CG, Parker TA, McMurry TJ, Brechbiel MW. Spectrophotometric method for the determination of a bifunctional DTPA ligand in DTPA-monoclonal antibody conjugates. *Bioconjug Chem.* 1992;3:342–345.

32. Gibaldi M, Perrier D. *Pharmacokinetics.* 2nd ed. New York, NY: Dekker; 1982.

33. Zhao B, Schwartz LH, Larson SM. Imaging surrogates of tumor response to therapy: anatomic and functional biomarkers. *J Nucl Med.* 2009;50:239–249.

34. Mankoff DA. Molecular imaging to select cancer therapy and evaluate treatment response. *Q J Nucl Med Mol Imaging.* 2009;53:181–192.

35. Horan Hand P, Colcher D, Salomon D, Ridge J, Noguchi P, Schlom J. Influence of spatial configuration of carcinoma cell populations on the expression of a tumor-associated glycoprotein. *Cancer Res.* 1985;45:833–840.

36. Di Nicolantonio F, Martini M, Molinari F, et al. Wild-type BRAF is required for response to panitumumab or cetuximab in metastatic colorectal cancer. *J Clin Oncol.* 2008;26:5705–5712.

37. Amado RG, Wolf M, Peeters M, et al. Wild-type KRAS is required for panitumumab efficacy in patients with metastatic colorectal cancer. *J Clin Oncol.* 2008;26:1626–1634.

38. Jimeno A, Messersmith WA, Hirsch FR, Franklin WA, Eckhardt SG. KRAS mutations and sensitivity to epidermal growth factor receptor inhibitors in colorectal cancer: practical application of patient selection. *J Clin Oncol.* 2009;27:1130–1136.

39. Cutler PD, Schwarz SW, Anderson CJ, et al. Dosimetry of copper-64-labeled monoclonal antibody 1A3 as determined by PET imaging of the torso. *J Nucl Med.* 1995;36:2363–2371.

40. Philpott GW, Schwarz SW, Anderson CJ, et al. RadioimmunoPET: detection of colorectal carcinoma with positron-emitting copper-64-labeled monoclonal antibody. *J Nucl Med.* 1995;36:1818–1824.